GEOPHYSICAL RESEARCH LETTERS, VOL. 21, NO. 4, PAGES 301-304, FEBRUARY 15, 1994

Teleseismic arrivals at a mid-ocean ridge: Effects of mantle melt and anisotropy

J-M. Kendall[1,2]

Abstract. Recent observational evidence of upwelling-mantle anisotropy at a slow spreading center has motivated the modeling of teleseismic arrivals at mid-ocean ridges. The models consider a variety of types of anisotropy and heterogeneity where the emphasis is to ascertain whether or not travel-times can be used to discriminate between the existence of partial melt and anisotropy. Two mechanisms for anisotropy in the upwelling asthenosphere are considered: one due to the preferential alignment of the fast axes of olivine crystals in the direction of mantle flow and the other due to the preferential alignment of cracks that feed melt towards the spreading axis. The results indicate that P-waves are most sensitive to even modest amounts of flow-induced asthenospheric anisotropy, while S-waves are most sensitive to the presence of mantle melt. Multiple S-wave arrivals are predicted for many models, most notably the ones with anisotropy due to crack-alignment where very large S-wave separations develop. The model which best fits existing data requires a higher degree of crystal-alignment anisotropy in the upwelling-asthenosphere than in the lithosphere. This effect has been predicted in studies of the evolution of crystal-alignment anisotropy in polycrystalline aggregates.

Introduction

In the early 1960's Hess [1964] showed clear evidence of upper-mantle P-wave anisotropy beneath oceans and attributed this to the alignment of olivine crystals in the direction of plate spreading. Since that time much effort has been devoted to studying anisotropy in the oceanic lithosphere using controlled-source experiments [e.g. Raitt et al., 1969] and global seismic studies using surface waves [e.g. Forsyth, 1975]. Concurrently, models of flow at spreading centers have provided a mechanism for crystal alignment in oceanic lithosphere [e.g. Ribe, 1989]. While the emphasis of this research has been anisotropy within lithosphere formed at a mid-ocean ridge (MOR), the possibility of anisotropy within the asthenospheric upwelling region at a spreading center has received very little attention.

The possible existence of anisotropy within the upwelling region at a MOR has been discussed by Phipps Morgan [1987] and Forsyth [1992]. In a recent study, Blackman et al. [1993] observed compelling evidence of anisotropy within the upwelling region of a portion of MOR. Anomalously early arrivals from teleseismic earthquakes were recorded by ocean bottom seismometers (OBS) situated across the ridge axis. Travel-time residuals increased with OBSs situated progressively further from the ridge. This result is somewhat counter-intuitive as the presence of partial melt at a MOR will slow seismic velocities. It is difficult to explain these observations without invoking anisotropy in the upwelling region. As in the lithosphere, this upwelling anisotropy is attributed to the preferential alignment of olivine crystals in the direction of material flow.

In an effort to quantify the degree of anisotropy required to explain the observations of Blackman et al. [1993] and to explore the trade-offs between anisotropy and partial melt at a spreading center, I have designed a series of ridge models which incorporate plausible estimates of anisotropy and heterogeneity.

The Models

The models considered are three-dimensional, but symmetric along strike, and represent the large-scale structure of a spreading center. Complexities due to crustal structure have been neglected as teleseismic arrivals are not high enough in frequency content to resolve such detail. Two generic ridge models are considered: a fast-spreading center (8cm/yr) and a slow-spreading center (1cm/yr). It is assumed that the lithosphere thickens with the square-root of age. The P-wave velocity contrast across the asthenospheric/lithospheric interface is assumed to be very small (7.9 to 8 km/s), while the S-velocity contrast is slightly larger (4.4 to 4.6 km/s). For simplicity, velocities above and below this interface are assumed to be constant.

Heterogeneity and anisotropy are added to each generic ridge model for five possible cases. The reference model is isotropic and has no velocity anomaly associated with melt. In the second case the effects of partial melt are included for a triangular-shaped (60km deep and 120km wide at the base, Figure 1) melt region consistent with passive upwelling. Following Faul et al. [1992] it is assumed that a plausible melt fraction for such a region would reduce P-wave velocities by 2% and S-wave velocities by 4%. It should be noted that S-waves will be very sensitive to the nature of the melt distribution and that much higher S-velocity reductions may be possible [Faul et al. 1992]. Also, melt fraction in the active-flow case will be much higher (up to 10% for P-waves), but confined to a very narrow upwelling region [Buck & Su 1989]. The third case assumes 7% P-wave anisotropy due to olivine alignment in the lithosphere, which is in agreement with measured values [e.g. Raitt et al., 1969]. The fourth and fifth cases include mechanisms for anisotropy in the asthenospheric upwelling region.

Anisotropy in the oceanic lithosphere is attributed to the lattice preferred orientation of olivine crystals at the time of accretion at a spreading center [Ribe, 1989]. It is argued that strong flow-velocity gradients in this region cause crystal orientation along the dominant glide system [001](100) which aligns the fast P-wave a-axis in the direction of spreading while the slow P-wave b-axis aligns in the vertical direction (Figure 1)

[1] IGPP, Scripps Inst. of Oceanography, UCSD
[2] now at: Dept. of Physics, University of Toronto

Paper number 93GL02791
0094-8534/94/93GL-02791$03.00

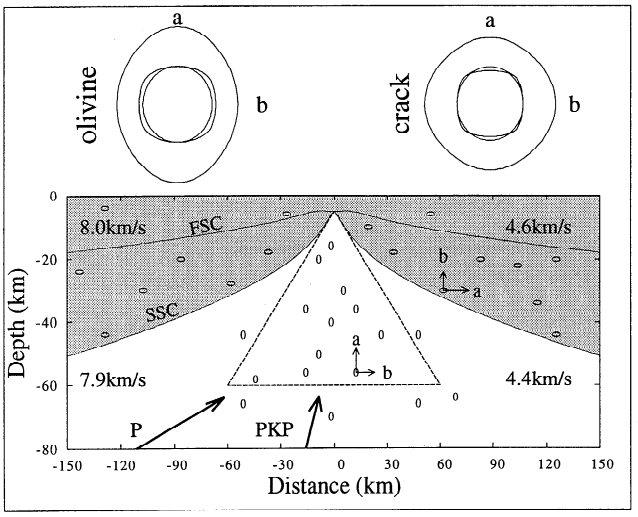

Fig. 1. A schematic diagram of the models considered. Shaded region indicates the lithosphere for a slow and fast spreading center (FSC and SSC). P-wave velocities are given on the left and S-wave velocities on the right. Ellipses show regions of anisotropy and the dashed triangle shows the region of partial melt for the passive flow case. Above the cartoon are the wave surfaces for a single olivine crystal (orthorhombic symmetry) and those for the region with vertically-aligned cracks (hexagonal symmetry). The outer surface is the P-wavefront propagating away from a point source and the inner surfaces are those for the fast and slow S-waves. The a- and b-axes for the wave surfaces and their orientation in model region are indicated.

[Estey & Douglas, 1986]. If strong flow gradients also exist in the upwelling region, similar crystal orientation could occur, but with the a-axis aligned in the vertical and the b-axis aligned perpendicular to the plane of the ridge axis (Figure 1). The percent anisotropy will decrease off-axis as flow-velocity gradients diminish. A cosine taper is therefore applied to the anisotropy distribution such that the model is isotropic 90km from the center of the upwelling. As a first guess, the degree of anisotropy at the center of the upwelling is assumed to be the same as that for the oceanic lithosphere (7%). Scaled versions of the 9 independent elastic constants of a single orthorhombic olivine crystal [Kumazawa & Anderson, 1969] are used to describe this anisotropy. The degree of alignment is controlled by mixing the background isotropic parameters with the parameters for the olivine crystal such that the starting models have roughly 7% P- and S-wave anisotropy [Kendall & Thomson, 1993].

An alternative mechanism for seismic anisotropy in the upwelling region is the preferential alignment of cracks or films. As noted by Faul et al. [1992], variations in the geometry of melt inclusions may significantly effect the S-wave velocities. The scenario is further complicated if these inclusions have a preferred orientation making the region anisotropic. If melt propagates up to the ridge axis through a network of thin dikes [Sleep, 1984] or films [Phipps Morgan, 1987] and there is a preferred alignment of these tabular structures, possibly due to regional stress fields, the medium as a whole will exhibit seismic anisotropy. This effect is well documented in fractured hydrocarbon reservoirs [e.g. Mueller, 1991]. The model assumes that the crack faces are aligned parallel to the plane of the ridge axis. As with the crystal alignment scenario, the percent anisotropy is assumed to decay away from the center of the upwelling region where most of the melt will be concentrated. As a first guess, the 5 independent elastic constants for the hexagonally-symmetric upwelling region are scaled versions of those given in Shearer & Chapman [1988] for a medium with fluid-filled elliptic cracks. The crack density is $\epsilon = 0.1$, the crack aspect ratio is 0.001 and the P-velocities in the cracks are 1/3 of those in the host medium. 3.5% P-wave anisotropy and 11% S-wave anisotropy results.

It should be noted that velocity effects due to changes in temperature and composition at a ridge have been neglected. These effects are considered to be second order in comparison to those due to partial melt and anisotropy [Cordery & Phipps Morgan, 1993].

Travel-time Predictions

Seismic rays are traced through the models using a ray tracer that calculates travel-times and amplitudes for 3D models with arbitrary anisotropy and curved interfaces [Guest & Kendall, 1993]. Rays are first traced to teleseismic distances through a 1D reference Earth model and then traced through the ridge models using the initial conditions provided by the global ray tracing [Kendall & Thomson, 1993]. P- and S-wave travel-times through fast and slow spreading centers for lower-mantle turning phases and core phases are shown in Figures 2–4. For these examples, rays are confined to the plane perpendicular to the ridge axis.

The isotropic fast-spreading model shows little variation (0.03 sec) in PKP travel-times due to the small amount of lateral heterogeneity (I in Figure 2a). Anisotropy in the lithosphere delays the arrivals slightly (L in Figure 2a) as the slow olivine b-axis is aligned vertically in this region (see Figure 1). The most significant travel-time effect is due to crystal-alignment anisotropy in the upwelling asthenosphere (0.4 sec earlier than the isotropic case, A in Figure 2a). The maximum travel-time delay due to passive-flow partial melt is 0.15 seconds (M in Figure 2a). The model with combined asthenospheric crystal-alignment anisotropy and partial melt clearly shows that the anisotropy produces the dominant travel-time effect. The active-flow case (not shown) with a higher melt-fraction, but confined to a narrower region, predicts that the melt effect may be quite strong, but only in a very narrow axial region. Ascribing the partial melt as a crack anisotropy gives no noticeable travel-time effects for nearly vertically traveling P-waves as only the near horizontal P-wave velocities are substantially affected by the vertically-aligned cracks (C in Figure 2a).

The travel-time effects for a PKP-phase at a slow-spreading center (Figure 2b) are qualitatively similar to those of the fast-spreading model. The travel-times for the isotropic model show more variation across the ridge axis reflecting the greater variation in lithospheric thickness for this model (see Figure 1). Accordingly, lithospheric anisotropy gives larger travel-time delays than those for the fast-spreading case. The interplay between the effects of lithospheric structure and the upwelling crystal-alignment anisotropy yields a triangular shaped travel-time pattern.

Asymmetrical travel-time patterns emerge when considering lower-mantle P-phases (Figures 2c). As with the PKP-arrivals, asthenospheric crystal-alignment anisotropy has a dominant travel-time effect over that due to the partial melt. The effect of asthenospheric crack

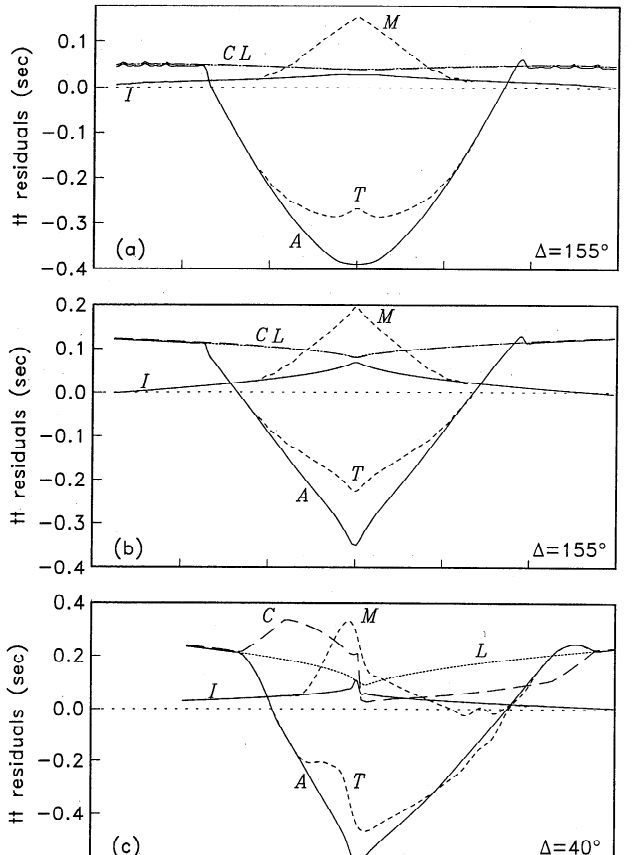

Fig. 2. The residual travel-time curves for P-waves: I for the isotropic model, M for the isotropic passive-flow model with a -2% velocity anomaly due to partial melt, L for the model with anisotropy only in the lithosphere, A for crystal-alignment anisotropy in the lithosphere and upwelling asthenosphere, C for anisotropy in the lithosphere and crack anisotropy in the upwelling mantle and T for crystal-alignment anisotropy in the lithosphere and upwelling region plus a -2% velocity anomaly due to partial melt. (a) Fast spreading center PKP-arrivals with an epicentral distance of 155°. Rays enter the local model with angles of incidence 5° off the vertical. (b) Slow spreading center PKP-arrivals. (c) Slow spreading center P-arrivals with an epicentral distance of 40°. Rays enter the local model with angles of incidence 30° off the vertical.

anisotropy is now discernible as there is a larger horizontal component in the raypaths for this phase. In general the travel-time residuals are larger for the P-phase than they are for the PKP-phase due to longer transit times through the models.

In general, two shear waves will propagate in an anisotropic medium. These shear waves will each spawn two more shear waves upon entering a second anisotropic medium. To complicate matters further, S-wavefronts in anisotropic media often exhibit wavefront cusps giving rise to travel-time triplications, although this is not a problem in the cases considered here (see wave surfaces in Figure 1). As a result, even very structurally simple models can generate a multitude of S-phases. To simplify the presentation of the S-wave travel-times for the ridge models only the fastest and slowest S-arrivals for a given model are shown in Figure 3. As a whole, the S-wave travel-time residuals are larger than those for the P-waves. In contrast to the P-waves results, the partial melt has the strongest effect on S-travel-times due to the inability of melt to support shear stresses. In reality this effect may be even more dramatic as the degree of S-velocity reduction may be much more than the minimum case scenario discussed here [Faul et al., 1992]. Crystal-alignment anisotropy in the upwelling region has a comparatively small travel-time effect for S-waves and the degree of SKS separation is very small for near vertically traveling rays (Figure 3). This is because the two SKS-waves propagate nearly vertically with velocities that are each essentially the isotropic value (see wave surfaces in Figure 1), an effect independent of percent anisotropy. Arrivals with larger ray parameters will start to show S-wave separations.

The S-wave travel-time residuals for the models with asthenospheric crack anisotropy are worth considering separately. Figure 4 shows the four possible shear arrivals for a slow spreading model with crack anisotropy in the upwelling region and crystal-alignment anisotropy in the lithosphere. The maximum degree of separation is very large (over 2.5 sec) due to the significant effect of partial melt on S-wave travel-times. The slow shear-wave in the fractured region possesses particle motion perpendicular to the fracture planes and is therefore very sensitive to the degree of cracking. In contrast, the faster shear-wave is polarized parallel to the crack faces and is less sensitive to the cracks. It should be emphasized that the crack model is somewhat arbitrary; variations in crack aspect ratio, density and fluid velocity will not change the symmetry of the anisotropy, but will scale the degree of S-wave separation. Comprehensive exploration of this parameter space would be required should shear-wave birefringence be observed in data.

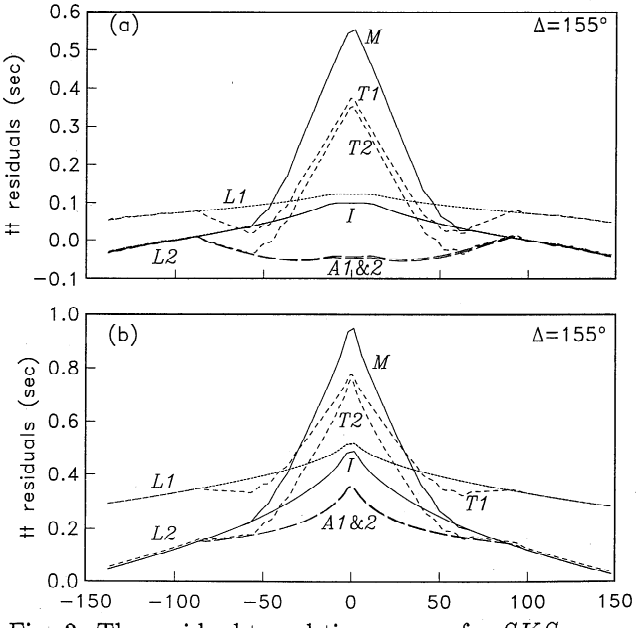

Fig. 3. The residual travel-time curves for SKS-waves at fast (a) and slow (b) spreading centers. See Figure 2 caption for details. There is a 4% velocity reduction in the melt region for cases M and T. The numbers following the letters indicate that there are two quasi-orthogonally polarized S-wave arrivals (e.g. L1 & L2).

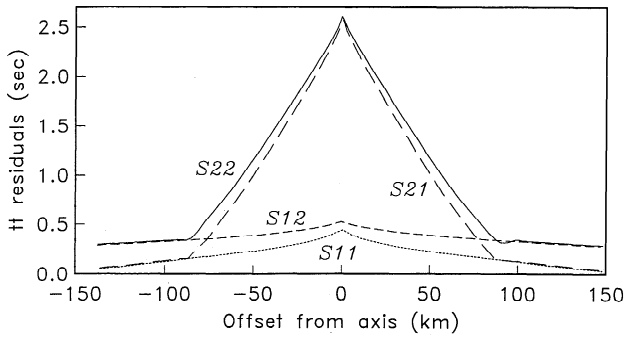

Fig. 4. The four residual travel-time curves for a SKS-phase at a slow spreading center with crystal-alignment anisotropy in the lithosphere and crack anisotropy in the mantle-upwelling region. $S11$ and $S22$ refer to arrivals that propagate as the respectively fast and slow shear waves throughout the models. Arrivals that travel as fast shear-waves through the asthenosphere and a slow shear-waves through the lithosphere are labeled $S12$ and *vice versa* for $S21$.

Comparison with Data

In Blackman et al. [1993] the results of this modeling are compared with data recorded at 34°S on the Mid-Atlantic Ridge, a site of slow spreading. Two PKP, one P and two PP phases from three $> m_b 5.5$ earthquakes were recorded on OBSs. The model which best fits the data is one with 15% crystal-alignment anisotropy in the upwelling region and 7% anisotropy in the lithosphere (see Blackman et al. [1993] for further details). The percent anisotropy in the asthenospheric upwelling may reduce somewhat if the anisotropy is spread deeper or there is some strong horizontal crystal-alignment off axis. Nevertheless, for realistic models a high degree of upwelling anisotropy is still required to explain the large travel-time residuals of Blackman et al. [1993]. It remains to be seen if this upwelling-mantle anisotropy is a global feature; perhaps this is a feature unique to slow spreading centers. Cordery & Phipps Morgan [1993] have shown, using models of plate and buoyancy driven flow and melt generation, that there may be very different flow gradients in upwelling regions at fast versus slow spreading centers. It is interesting that the results require a significantly higher degree of anisotropy in the upwelling region than in the lithosphere. A single crystal of olivine has ≈25% P-wave anisotropy. In order to get 15% anisotropy in the upwelling olivine-rich peridotite, there must be a substantial degree of crystal alignment. Using a finite-element formulation based on polycrystalline theory to describe the plasticity in mantle minerals, Chastel et al. [1993] have shown that this effect is perhaps not unexpected. Upwelling mantle material may have a higher degree of crystal orientation than that in material that subsequently travels horizontally. Future seismic modeling in conjunction with such geodynamical modeling will provide important insights into melt and flow processes beneath a mid-ocean ridge.

Acknowledgements. The author thanks Drs. D. Blackman, J. Orcutt, J. Phipps Morgan, R. Evans and an anonymous reviewer for helpful advice and comments. This work was supported by a NSERC Canada Postdoctoral Fellowship and the Cecil and Ida Green Foundation.

References

Blackman, D. K., J. A. Orcutt, D. W. Forsyth & J-M. Kendall, Seismic anisotropy in the mantle beneath an oceanic spreading center, in press *Nature*, 1993.

Buck, W. R. & W. Su, Focused mantle upwelling below mid-ocean ridges due to feedback between viscosity and melting, *Geophys. Res. Lett., 16*, 641-644, 1989.

Chastel, T. B., Dawson, P. R., H-R. Wenk & K. Bennett, An anisotropic model for the upper mantle, *J. Geophy. Res., 98*, 17757-17771, 1993.

Cordery, M. J. & J. Phipps Morgan, Convection and melting at mid-ocean ridges, in press *J. Geophys. Res.*, 1993.

Estey, L. H. & B. J. Douglas, Upper mantle anisotropy: a preliminary model, *J. Geophys. Res., 91*, 11393-11406, 1986.

Faul, U. H., D. R. Toomey & E. Humphreys, Seismic imaging of the east Pacific rise upper mantle: forward and inverse modeling of body wave data, *RIDGE report*, 1992.

Forsyth, D. W., The early structural evolution and anisotropy of the oceanic upper mantle, *Geophy. J. R. astr. Soc, 43*, 103-166, 1975.

Forsyth, D. W., Geophysical constraints on mantle flow and melt generation beneath mid-ocean ridges, in *Mantle flow and melt generation at mid-ocean ridges*, eds J. Phipps Morgan, D. K. Blackman, J. M. Sinton, *Amer. Geophys. Mon. Ser., 71*, 1-66, 1992.

Guest, W. S. & J-M. Kendall, Modeling waveforms in anisotropic inhomogeneous media using ray and Maslov theory: applications to exploration seismology, *Can. J. Expl. Geophys., 29*, 78-92, 1993.

Hess, H. H., Seismic anisotropy in the uppermost mantle under oceans, *Nature, 203*, 629-631, 1964.

Kendall, J-M. & C. J. Thomson, Seismic modeling of subduction zones with inhomogeneity and anisotropy, I: Teleseismic P-wavefront geometry, *Geophys. J. Int., 112*, 39-66, 1993.

Kumazawa, M. & O. L. Anderson, Elastic moduli, pressure derivatives and temperature derivatives of a single-crystal olivine and a single crystal forsterite, *J. Geophys. Res., 74*, 5961-5972, 1969.

Mueller, M. C., Predictions of lateral variability in fracture intensity using multicomponent shear-wave surface seismic as a precursor to horizontal drilling in the Austin chalk, *Geophys. J. Int., 107*, 409-416, 1991.

Phipps Morgan, J., Melt migration beneath mid-ocean spreading centers, *Geophys. Res. Lett., 12*, 1238-1241, 1987.

Raitt, R. W., G. G. Shor, T. J. G. Francis & G. B. Morris, Anisotropy of the Pacific upper mantle, *J. Geophys. Res., 74*, 3095-3109, 1969.

Ribe, N. M., Seismic anisotropy and mantle flow, *J. Geophys. Res., 94*, 4213-4223, 1989.

Shearer, P. M. & C. H. Chapman, Ray tracing in anisotropic media with a linear gradient, *Geophys. J. Int., 94*, 575-580, 1988.

Sleep, N. H., Tapping of magmas from ubiquitous mantle heterogeneities: An alternative to plumes?, *J. Geophys. Res., 89*, 10029-10041, 1984

J-M. Kendall, Department of Physics, University of Toronto, Toronto, Ontario, Canada M5S 1A7.

(Received August 9, 1994; accepted October 4, 1993)